https://doi.org/10.22226/2410-3535-2022-4-360-366

Mechanical properties of Al-Nb *in situ* metal-matrix composites fabricated by constrained high pressure torsion at 10 GPa and subsequent annealing

K. S. Nazarov[1], G. F. Korznikova[†,1], R. Kh. Khisamov[1], R. R. Timiryaev[1], E. A. Korznikova[1,2,3], G. R. Khalikova[1,3], R. U. Shayakhmetov[1], S. N. Sergeev[1], R. R. Kabirov[1], R. R. Mulyukov[1,3]

[†]gfkorznikova@gmail.com

[1]Institute for Metals Superplasticity Problems, RAS, Ufa, 450001, Russia
[2]Ufa University of Science and Technology, Ufa, 450008, Russia
[3]Ufa State Petroleum Technological University, Ufa, 450062, Russia

Mechanical alloying of dissimilar metals by means of severe plastic deformation techniques is known to be a perspective method of obtaining *in situ* metal matrix composites with advanced properties. Recent investigations found out that besides severe mixing of elements, intensive formation of non-equilibrium intermetallic phases takes place. Presence of intermetallic particles in the composite affects both its physical and mechanical properties. In this work we have realized the fabrication of Al-Nb composites in one step by means of high-pressure torsion technique. A non-trivial phenomenon of growth of tensile strength with increasing number of revolutions during HPT was revealed. It was explained by more homogeneous mixing of components and precipitation of intermetallic phase in the vicinity of Al-Nb interphases. The microstructural observations and X-ray diffraction analysis allowed to reveal Al_3Nb intermetallic phase in the as deformed composites, while the equilibrium temperature of formation of this phase is above 600°C. Varying the number of revolutions and post deformation annealing allows obtaining composites with different fractions of intermetallic particles. This approach can be considered as a way for the development of composites with a tailorable complex of physical and mechanical properties.

Keywords: metal matrix composites, high pressure torsion, interface bonding, phase transformations, mechanical properties.

1. Introduction

In recent years, more and more attention has been attracted to metal-matrix composites (MMC) due to their improved physical and mechanical properties in comparison with the properties of pure metals [1]. For example, in pursuit of lightweight and high-performance materials for various applications Al-based composites were proven to be an outstanding candidate for replacement of conventional alloys due to their superior mechanical, tribological, electrical, corrosion resistance and thermal properties compared to those of base alloys [2 – 4]. The properties and performance of MMCs are normally determined by the nature and morphology of its counterparts and are controlled by the nature of the matrix-reinforcement interfaces. From the point of view of the interaction of the composite's constituents, one can differ *in situ* and *ex situ* composites [5,6] by the conjugacy type of the matrix and reinforcement. *Ex situ* composites having incorporated particles with an incoherent interface with respect to the structure of the matrix are normally characterized by enhanced strength and operation temperature of the material [6]. However, in a number of cases, they are inferior to *in situ* composite materials with coherent types of matrix/precipitate interfaces in such properties as ductility, long-term strength, and structure tailoring ability [3,6]. Severe plastic deformation techniques involving very large strains typically involving a complex stress state or high shear, resulting in a high defect density [7] was found to be an effective tool for managing size, morphology and volume fraction of reinforcement particles defining the properties of the final product. It is also known for its ability to promote the solid-state reactions. For instance, in [8] it was shown that the estimated diffusion coefficients during HPT processing appear to be up to 10^{22} times higher than lattice diffusion and can even be compared to surface diffusion.

A particular case of severe deformation, high-pressure torsion (HPT), has recently been discovered to be an effective way for the synthesis of in situ metal matrix composites. In this method, a disk or a set of discs to be strained is placed between 2 anvils. Large compressive stress and special type of anvils used allows to reach huge amount of strain without fracture [7]. This approach has been successfully used for formation of homogeneous composite structures in Al-Mg [9,10], Al-Cu [11–13], Al-Ti [14,15], and various other systems including even such a dissimilar combination as Al-Nb [16]. It should be noted that most composites consisting of metals with

very different melting points and strength characteristics, such as Al-W [17] and Al-Ti [18], were obtained only by powder consolidation. Most studies of Al-based HPT-synthesized disc composites were focused on moderately dissimilar Al-Mg [9,10] Al-Cu [11–13] Al-Ni [19] and other kindred systems. The ability to obtain uncontaminated metal matrix composites from highly dissimilar metals may open new prospects for the development of new materials with enhanced properties. HPT-processed composite materials combining the high strength of an intermetallic constituent with the ductility of a pure metal is one of the obvious ways to obtain new types of composites due to the defect-mediated diffusion, which promotes the formation of an intermetallic phase significantly below the equilibrium temperature. An example of such combination is the Al-Nb system, which allows one to benefit from both the light weight of Al and high strength of Nb in frames of creation of a composite with an attractive set of properties [20]. This work is focused on the synthesis of Al-Nb composites by means of solid-state welding of thin discs and analysis of their mechanical properties and post deformational annealing behavior.

Previous experiments on HPT-induced solid state joint in Al-Nb composites resulted in formation of a bulk composite structure after 30 revolutions under the pressure of 6 GPa [14], while in Al-Cu and Al-Mg composites a bulk composite structure was obtained after ten [12] or even five [9] revolutions. However, due to the large difference between the hardness of Al and Nb, 10 revolutions of the HPT anvil were not enough to obtain a bulk composite structure, since most of the shear deformation was dissipated through the ductile aluminum counterpart, which prevented the refinement of Nb and the mutual mixing of the components.

The current study is a continuation of the work on the deformation-induced production of Al-Nb MMC. The aim of this work was to obtain a monolithic metal matrix composite of the Al-Nb system with inclusions of intermetallic particles by direct conjunction of pure Al and Nb discs under the pressure 10 GPa using 30 and 100 revolution of anvil and to analyze the evolution of the microstructure and tensile properties of the composites upon annealing.

2. Materials and experimental methods

The initial billets of metals were aluminum (99.5%) and niobium (99.9%). To obtain samples of the Al-Nb composite by constrained HPT, anvils with a diameter 12 mm and grooves with a total depth 0.5 mm were used. Constrained HPT processing was applied to a set of 3 disks with the alternation of layers, i.e. plate of hard Nb was placed between two plates of soft Al, which leads to better mixing of metal layers [15]. The thickness and diameter of Al were 1 and 10 mm, and that of Nb, 0.3 and 12 mm, respectively, which means an Al content of 57.64 wt.% (82.41 at.%), and Nb content of 42.36 wt. % (17.59 at.%). The pressure during the torsion was 10 GPa and kept constant with a deformation rate of 3 revolutions per minute at room temperature. The resulting samples had the form of disks 12 mm in diameter and 0.7 mm thick.

Obviously, Nb has a higher hardness than Al and its fragmentation, dispersion, and distribution over the volume of the composite sample requires a greater strain, which in turn means a greater number of rotations of the anvil. Considering this, the number of revolutions of the anvil was increased to n=100 to obtain the maximum fraction of the mixed structure. For comparison, samples with a number of revolutions of n = 30 were also processed.

It was earlier shown by means of differential thermal analysis that strain-induced formation of the Al_3Nb intermetallic compound in HPT processed MMCs occurs mainly in the interval 300 – 400°C [16]. Therefore, to form intermetallic phases, Al-Nb MMCs with revolution numbers n = 30 and n =100 were annealed at 400°C for 10 minutes.

The study of the microstructure and the measurement of microhardness were carried out on the cross section of the samples (see the cutting scheme in Fig. 1). The cross section of the samples was preliminarily subjected to mechanical grinding and polishing to give a mirror-smooth surface. The microstructure and homogeneity of the distribution of metal layers on the sample surface were studied using Tescan Mira 3LHM scanning electron microscopy (SEM) equipped with an EDX detector. Transmission electron microscopy studies were performed on the JEM 2100 Plus at 200 kV accelerating voltage. The selected area diffraction pattern was taken from a 2 μm² area. The phase composition was studied with a high-resolution Rigaku Ultima IV X-ray diffractometer using Cu-K_α radiation. The phase content was quantified by Rietveld analysis. Rietveld refinement was utilized in MAUD software, using harmonic model for texture accounting. TEM and XRD samples were cut from the middle layer indicated by blue in Fig. 1a.

The microhardness was measured by the Vickers method using an MHT-10 microhardness tester combined with

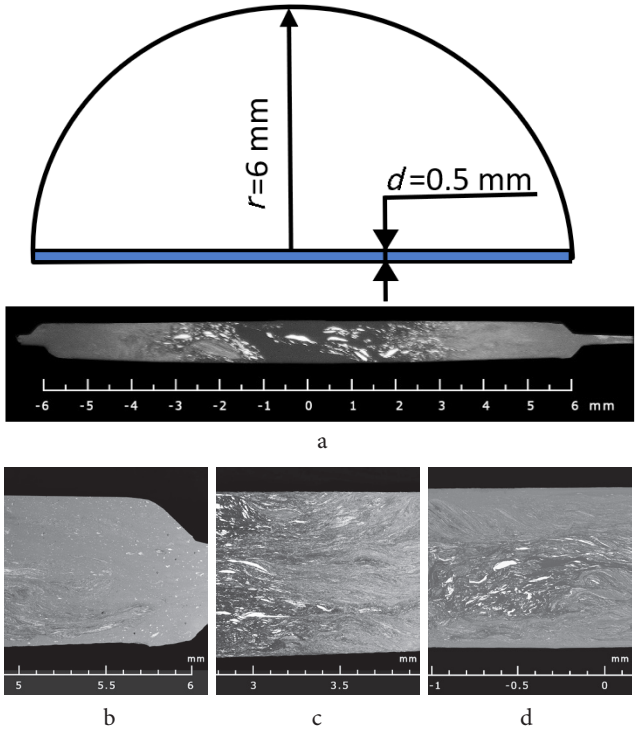

Fig. 1. SEM (BSE mode) images of Al-Nb composite cross-section HPT, P=10 GPa, n = 30: disc cutting pattern and the full view (a), edge area (b), mid radius area (c), central area of the sample (d). Dark and bright contrast correspond to pure aluminum and niobium respectively.

a Carl Zeiss optical microscope. The load was set to 50 g (0.4903 Newtons). First, microhardness measurements were carried out on the sample in the as deformed state, then the sample was annealed, and measurements were taken again on the same sample. For comparison, the microhardness of the initial billets of aluminum and niobium was measured, as well as the microhardness of the HPT processed aluminum and niobium (n=10).

Tensile strength tests were carried out on a CMT-5 tensile testing machine (Liangong Testing Technology Co.). From disk samples with a diameter of 12 mm two specimens were cut from the middle radius zone dumbbell-shaped samples were cut out in the area between the center and the edge of the sample. The gauge length and width were 3 and 1 mm respectively and corresponded to a portion of the disk sample located approximately 3 mm from its edge. Tensile tests were conducted using specially elaborated locks [21] mounted in tensile testing machine. The tests were carried out at room temperature with a strain rate of 0.5×10^{-1} s^{-1} until fracture of the specimen. Four specimens were tested for each structural state.

3. Results and discussion

3.1. Microstructure in the as-deformed state

As a result of deformation by constrained HPT at 10 GPa monolithic samples of Al-Nb composites were obtained. Microstructure observations show that at relatively low number of revolutions, the homogeneity of the mixing of the aluminum and niobium layers occurs predominantly at the edge of the sample. With an increase in the number of revolutions, the homogeneity of mixing of the metal layers extends from the edge to the central part of the sample.

The cross-sectional structure of the Al-Nb sample, obtained at the number of revolutions n=30, is presented in Fig. 1. The white region on the micrographs represents a Nb-rich phase and the gray region represents the Al-based phase. A gradient structure was formed in the sample with a gradual decrease in the size of structural components from the center to the edge what is related to growth of the deformation degree upon distancing from the center. Three zones in the center, zone at the middle of the disc radius area hereinafter mentioned as mid-radius, and at the edge of the samples with a representative structure type were selected for analysis. The highest mixing degree accompanied by formation of the homogeneous lamellar free nanostructure is located in the vicinity of the sample edge (Fig. 2 b). Only a few small areas with laminated structure are observed in the periphery region as well as separate small inclusions of Nb. The chemical composition of this area (see supplementary materials, Fig. S1), analyzed by EDX, averages: aluminum — 90%, niobium — 10% (at.%). Nanolaminated structure is observed in the area close to the middle of the radius (Fig. 2 c, more detailed image at higher magnification presented in supplementary materials, Fig. S2). The thickness of alternate lamellas of Nb and Al is less than 500 nm. The originally flat interface between Al and Nb layers transforms and bending and vortice-type foldings are formed. The formation of vortices is a result of instabilities of interfaces between dissimilar metals caused by local blocking of shear deformation, as it has been discussed recently in [13]. An additional driver for interface instabilities can be the formation of intermetallic phases during HPT [22]. The structure of the central part of the sample consists mainly of aluminum with large single inclusions of niobium (Fig. 1d).

The structure of the Al-Nb MMC fabricated at the number of revolutions n=100 seems to be more uniform (Fig. 2 a) and differs significantly from the structure of the Al-Nb MMC processed with n=30. At the edge of the sample, as well as at the edge of the Al-Nb sample (n=30), homogeneous lamellar free nanostructure with small inclusions of Nb in Al is observed (Fig. 2 b). Similar structure appeared in the vicinity of the upper and lower parts of the entire disk (top and bottom in Fig. 2 a, c, d). In mid-radius area (Fig. 2 c) the structure of the Al-Nb MMC (n=100) consists entirely of curved Nb-rich and Al-rich layers. In the central area of the sample, individual thin inclusions of niobium in aluminum are observed (Fig. 2 d).

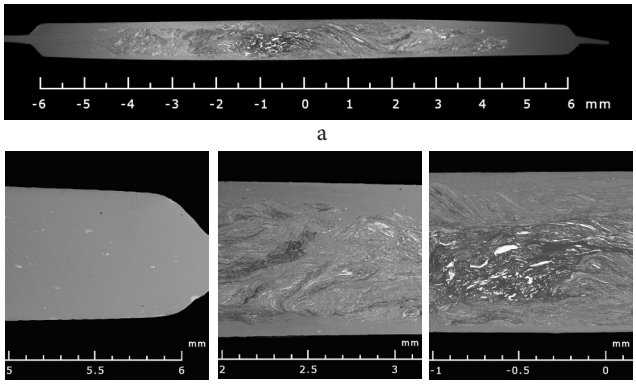

Fig. 2. SEM images of cross-section HPT Al-Nb sample, P=10 GPa, n=100: full view (a), edge area (b), mid radius area (c), central area of the sample (d).

3.2. Deformation induced and annealing induced phase transformations

The structure of both composites annealed at 400°C is not significantly different from those of the as-deformed ones evaluated by SEM observations. Table 1 shows the phase composition of Al-Nb composites fabricated by HPT with revolution numbers n=30 and n=100, as well as of the composites annealed at 400°C for 10 minutes detected by X-ray diffraction analysis. As can be seen, the composites contain 60÷65% aluminum and 30÷35% niobium, which is consistent in composition with the stacking scheme of Al-Nb-Al stacks during deformation, i.e., corresponds to relation 2:1. At the same time this relation differs slightly from the initial one, which is associated with the outflow of

Table 1. Phase composition of the HPT Al-Nb composite in the as deformed state and after annealing.

Composite	Al (wt.%)	Nb (wt.%)	Al_3Nb (wt.%)
n=30	64.7	32.5	2.8
n=30, T=400°C	63.0	31.4	5.0
n=100	59.5	30.5	10.0
n=100, T=400°C	56.6	28.4	15.0

part of the material outside anvils. Both composites in the as deformed state are primarily composed of crystalline fcc Al-rich and bcc Nb-rich phases along with some amount of tetragonal intermetallic Al_3Nb phase. The fraction of Al_3Nb intermetallic phase increased upon the growth of the strain degree. Strain-induced formation of Al_3Nb intermetallic phase at room temperature was reported in our previous paper [14]. An increase in the fraction of Al_3Nb phase with an increase in the number of revolutions is due to enhanced mechanical mixing of the components and an increase in the number of interphase boundaries of aluminum and niobium in the sample, what contributes the mechanical mixing of components and subsequent intermetallic phase formation. It should also be noted that the temperature of the anvil, measured by an infrared camera, increases during HPT processing and reaches 100°C (see supplementary materials, Fig. S3). But this temperature remains lower than the equilibrium temperature of formation of Al_3Nb phase. Apparently, the Al_3Nb phase is formed predominantly in homogeneous nanocrystalline structure that has arisen in the areas of homogeneous mixing in the Al-Nb composite with $n=100$ revolutions, which is significantly larger than that of the Al-Nb sample with $n=30$, as shown by SEM studies (Fig. 1, 2).

Table 2 shows the data obtained from the analysis of the broadening of the XRD profiles of Al (see supplementary materials, Fig. S4). It can be seen that the lattice parameter in both as-deformed states are higher than that in undeformed ($n=0$) Al, which may be associated with the formation of a supersaturated solid solution and also with lattice distortion.

TEM observations confirmed the presence of Al_3Nb intermetallic phase in homogeneous nanocrystalline lamellar free area near the mid-radius of the composite in the as-deformed state (Fig. 3). Mostly, precipitates diameter does not exceed 20 nm, while grain size in this area is about 50 nm. Strain-induced formation of Al_3Nb intermetallic phase at low temperature is not a common fact since according to the equilibrium state diagram [23] the equilibrium temperature of formation of this phase is above 600°C.

Subsequent annealing reveals significant increase of the Al_3Nb fraction with the appropriate decrease of pristine elements (see Table 1). It should be noted that the annealing temperature of 400°C is also below the equilibrium temperature of 600°C. Most likely, an increase in the concentration of the Al_3Nb phase occurs due to decomposition of supersaturated solid solution of Nb in Al because of thermal activation of diffusion processes during post deformation annealing. TEM observations revealed significant grain growth and annihilation of the defects due to recrystallization of Al matrix during annealing (Fig. 3 c).

According the equilibrium state diagram [23], the Al-Nb system supports three intermetallic phases and the formation of only one intermetallic phase after the continuous annealing, as revealed here, is not a trivial fact. Similar result was obtained during mechanical alloying [24] and friction stir welding, [25] where the authors report the decrease of the Al_3Nb phase formation temperature from 933°C for initial powder mixture to 454°C after mechanical alloying. Formation of the single intermetallic phase instead of the three which present in the phase diagram was reported and explained in [16, 26] and caused by quite limited solubility of Nb in Al and the lowest value of the effective heat of formation for the Al_3Nb phase [27]. These arguments are supported as well by the XRD data [24].

Table 2. Lattice parameter, coherent scattering region, and lattice microstresses of Al-Nb composite samples obtained by shear deformation.

Composite	Lattice parameter, Å	Coherent-scattering region, nm	Lattice Microstresses $\times10^{-4}$
$n=0$	4.0499 ± 0,0003	560 ± 60	0.13 ± 0.07
$n=30$	4.0505 ± 0.0006	80 ± 4	6.3 ± 0.15
$n=30$, $T=400$°C	4.0503 ± 0.0006	105 ± 6	4.33 ± 0.14
$n=100$	4.0578 ± 0.0002	75 ±10	13.9 ± 0.3
$n=100$, $T=400$°C	4.0538 ± 0.0003	110 ±19	11.6 ± 0.5

3.3. Microhardness distribution and its evolution upon annealing

Measurements of the microhardness distribution along the diameter in the cross section of the Al-Nb composites were performed in the as- deformed state with $n=30$ and $n=100$ and after subsequent annealing at 400°C. Results are shown in Fig. 4. Every point is a result of averaging upon four measurements. Microhardness distribution in pure Al and Nb subjected to HPT is also presented for comparison. It is clearly seen that values of microhardness

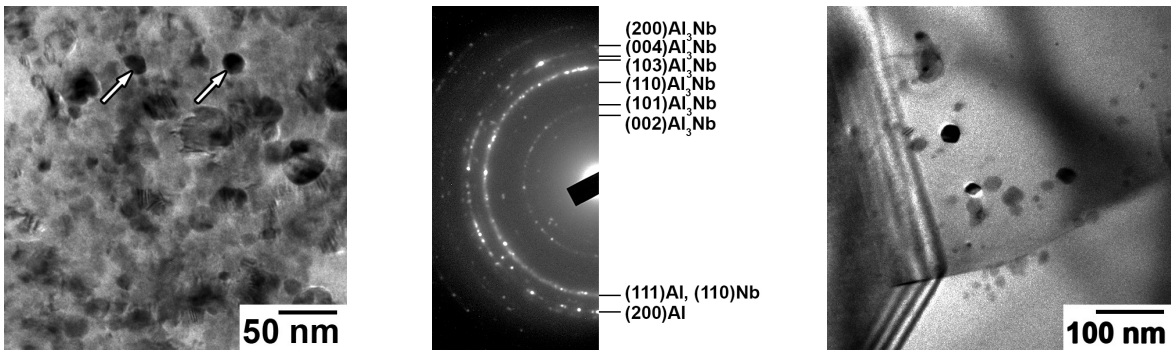

a b c

Fig. 3. Transmission electron microscope bright field image (a) and selected area diffraction patterns (b) of Al-Nb composite processed with $n=30$ in the as-deformed state (a, b) and after subsequent annealing (c). The foils were cut out of the mid-radius area. Arrows indicate some intermetallic precipitates of Al_3Nb.

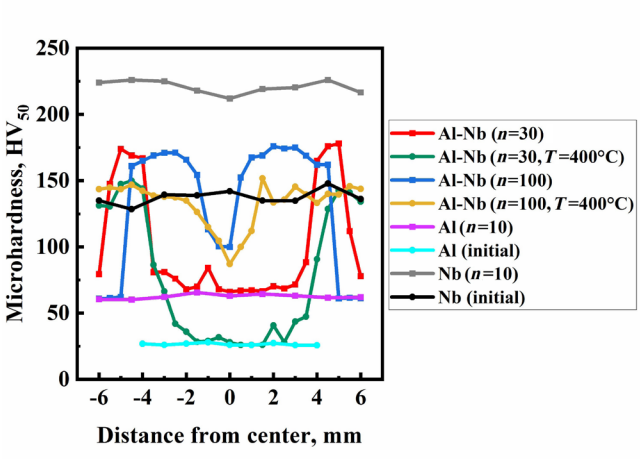

Fig. 4. (Color online) Microhardness of Al-Nb composites HPT processed with $n=30$ and $n=100$ and after annealing at 400°C for 10 minutes.

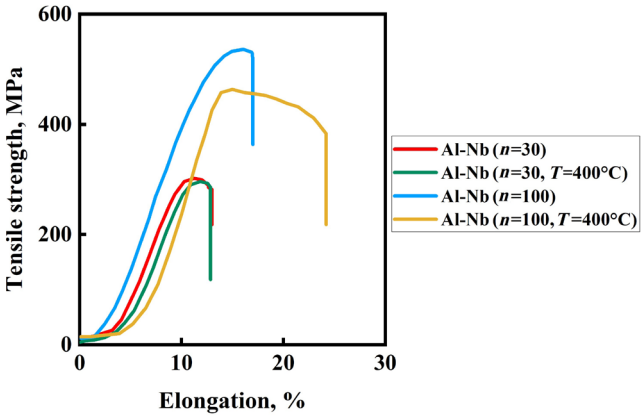

Fig. 5. (Color online) Fracture strength diagrams of HPT Al-Nb composites in the as-deformed state and after annealing.

of both as-processed composites are in the interval between microhardness values of Al HPT and Nb HPT.

An analysis of the distribution of microhardness of as-deformed Al-Nb MMCs shows that the latter does not follow the most common path of increasing microhardness with distance from the center, as was observed previously in HPT processed pure metals, alloys and some MMC [9]. At the edge of both as-deformed composites, the microhardness is about 60÷80 HV, which is close to the microhardness value of pure Al after HPT. The maximum value of microhardness ≈170 HV was observed in mid-radius area both for $n=30$ and $n=100$ and what is more in composite with $n=100$, the zone with increased microhardness extended almost to the center of the sample. Only in the small central part of the sample, the microhardness decreased to 100 HV. The microhardness value of the Al-Nb composite ($n=30$) with a coarse mixing zone in the center containing large fractions of pristine Nb and Al fragments, decreases almost to a level of the HPT processed Al.

Thus, the values of microhardness of HPT processed Al-Nb composites are consistent with their microstructure. Lower microhardness values were revealed to be located at the composite edges with homogeneous lamella free microstructure. The maximal degree of shear deformation on the edge results in the formation of the strain-induced homogeneous solid solution, which leads to decrease of the interface hardening. Emergence of nanolaminated structure with enhanced area of interphases in mid-radius area, in combination with the high density of defects contributes to a sharp growth of HV. Increase of deformation degree by increasing the number of revolutions from $n=30$ to $n=100$ during HPT processing results on extended area with high microhardness. In the central part of the composites according to microstructure analysis poor mixture and coarse fragments of Al and Nb phases are detected, defining the low microhardness in this region.

Annealing of the composites at 400°C results in the overall decrease of the microhardness due to annealing of HPT-induced defects. However, the values of the microhardness increased at the edge of the samples after annealing due to the formation of the Al_3Nb being the result of the enhanced diffusion in the solid solution region. On Al-Nb composite ($n=100$) after annealing at 400°C the microhardness over the entire cross section of the sample almost leveled off, except for a small central part with a diameter about 3 mm, and its value was about 125÷140 HV.

3.4. Tensile properties

Strength tests of HPT Al-Nb specimens are consistent with the results of microhardness measurements. The measured tensile strength values correspond to the microhardness values of the Al-Nb samples at a distance of 3 mm from the center. The HPT Al-Nb sample ($n=100$) has the highest strength, the tensile strength value is 530 MPa (Fig. 5). Annealing the sample HPT Al-Nb ($n=100$) at 400°C led to some decrease in the tensile strength to 470 MPa. HPT Al-Nb specimens ($n=30$) both before and after annealing at 400°C showed values of ultimate strength — about 300 MPa. In the tensile diagram of the samples, it can be seen that the samples show signs of plasticity. This is evidenced by some elongation before fracture. The HPT Al-Nb ($n=100$, $T=400$°C) sample showed the highest plasticity about 12% after annealing. A viscous fracture of this sample was observed by SEM (see supplementary material, Fig. S5). Clearly faceted grains of Al_3Nb intermetallic inclusions located in the Al-rich matrix are visible at high magnifications. Al-rich matrix remains viscous, as evidenced by dimples and curved fracture lines.

Previously [16, 28] we have demonstrated that severe plastic deformation using the pressure of 6 GPa and 30 revolutions, can promote solid-state reactions through direct bonding at room temperature of two dissimilar metals fcc Al and bcc Nb, the melting points of which differ by more than 3 times. Besides this formation of a small amount (≈3%) of Al_3Nb intermetallic phase was detected at room temperature deformation, while in this work, the state after $n=30$ revolutions at 10 GPA, contains ≈3% of Al_3Nb intermetallic phase, i.e. the increase in pressure did not lead to an increase in the content of Al_3Nb while its equilibrium formation normally occurs above 600°C. However, the resulting discs of the same thickness that in [14, 26] had poor mixing in a rather large central zone. The present work demonstrated that the increase in pressure up to 10 GPa and

torsional straining up to 100 revolutions of HPT anvil leads to a fair mixture of components, formation of large areas of homogeneous nanocrystalline structure and a significant fraction (≈10%) of HPT induced Al_3Nb intermetallic phase. The composite processed under mentioned conditions after annealing has rather homogeneous distribution of microhardness except for a small central part with a diameter less than 3 mm. Tensile tests demonstrated a considerable dependence of tensile strength on HPT straining which almost doubled upon the increase of torsional straining from 30 to 100 revolutions of HPT anvil. Another important result is high value of elongation to failure (≈12%) with a slight decrease in tensile strength after annealing of HPT Al-Nb composite processed with 100 revolutions.

Thus, HPT is a well-established approach for improvement of the components homogeneity due to mechanical mixing of components induced by huge shear strains during HPT, which can result in the formation of supersaturated solid solutions for metals which have limited solubility in each other in normal conditions. Additional contribution is related to increased density of lattice defects [8] and elevated effective temperature during HPT processing [29]. In turn it promotes the diffusion and facilitates the formation of a homogeneous structure and precipitation of HPT induced hardening Al_3Nb intermetallic phase. Al-Nb composites are known to have enhanced electrical properties by comparison to pure Al which along with the improved tensile strength and elongation to failure makes them a possible candidate for various electrotechnical and engineering applications.

4. Conclusions

1. Increase in pressure up to 10 GPa and torsional straining up to 100 revolutions of HPT anvil leads to a fair mixing of components and formation of large areas of homogeneous nanocrystalline structure with 10% of HPT induced hardening Al_3Nb intermetallic phase that increased to 15% after annealing at 400°C in HPT processed Al-Nb metal matrix composites.

2. Al-Nb metal matrix composite processed under 10 GPa and 100 revolutions of HPT anvil after annealing at 400°C has rather homogeneous distribution of microhardness except for a small central part with a diameter less than 3 mm.

3. Increase in torsional straining from 30 to 100 revolutions leads to an increase in strength from 300 to 530 MPa due to a fair mixing of components and higher fraction of HPT induced intermetallic phase. Post deformation annealing at 400°C leads to some decrease in strength down to 470 MPa, but a significant increase in ductility due to grains growth and defects annihilation in Al matrix.

Supplementary material. *The online version of this paper contains supplementary material (EDX data, Fig. S1, enlarged SEM image of nanolaminated structure, Fig. S2, images obtained by an infrared camera during SPD processing, Fig. S3, XRD profiles, Fig. S4, SEM images of fractography of HPT Al-Nb (n=100, T=400°C) composite after tensile test, Fig. S5) available free of charge at the journal's website (lettersonmaterials.com).*

Acknowledgments. The present work was accomplished according to the state assignment of IMSP RAS and supported by the Russian Science Foundation (Grant No. 18-12-00440-II). SEM studies were performed using the equipment of the Center for Shared Access "Structural and Physicomechanical Investigations of Materials" at the Institute for Metals Superplasticity Problems of Russian Academy of Sciences. The work of E. A. K. is supported within the framework of the work on the state assignment of the Ministry of Education and Science of Russia for the Federal State Budgetary Educational Institution of Higher Education "USATU" (agreement No. 075-03-2021-014/4) in the youth research laboratory "Metals and Alloys under Extreme Impacts" (discussions, conceptualization, contribution to the initial draft preparation).

References

1. N. R. Bandyopadhyay, S. Ghosh, A. Basumallick. Materials and Manufacturing Processes. 22, 679 (2007). Crossref
2. M. K. Surappa. Sadhana. 28, 319 (2003). Crossref
3. M. O. Bodunrin, K. K. Alaneme, L. H. Chown. J. Mater. Res. Techn. 4 (4), 434 (2015). Crossref
4. S. Mohapatra, A. K. Chaubey, D. K. Mishra, S. K. Singh. J. Mater. Res. Techn. 5, 117 (2016). Crossref
5. A. V. Aborkin, A. I. Elkin, V. V. Reshetniak, A. M. Ob`edkov, A. E. Sytschev, V. G. Leontiev, D. D. Titov, M. I. Alymov. Journal of Alloys and Compounds. 872, 159593 (2021). Crossref
6. R. Casati, M. Vedani. Metals. 4, 65 (2014). Crossref
7. R. Z. Valiev, R. K. Islamgaliev, I. V. Alexandrov. Prog. Mater. Sci. 45, 103 (2000).
8. K. Oh-ishi, K. Edalati, H. S. Kim, K. Hono, Z. Horita. Acta Materialia. 61, 3482 (2013). Crossref
9. M. Kawasaki, J.-K. Han, D.-H. Lee, J. Jang, T. G. Langdon. J. Mater. Res. 33, 2700 (2018). Crossref
10. M. Kawasaki, J. Jang. Materials. 10, 596 (2017). Crossref
11. J. K. Han, G. Y. Liang, M. Kawasaki, D. K. Han, J. I. Jang, T. G. Langdon. Adv. Eng. Mater. 20 (11), 1800642 (2018). Crossref
12. G. F. Korznikova, K. S. Nazarov, R. Kh. Khisamov, S. N. Sergeev, R. U. Shayachmetov, G. R. Khalikova, J. A. Baimova, A. M. Glezer, R. R. Mulyukov. Mater. Lett. 253, 412 (2019). Crossref
13. R. Kulagin, Y. Beygelzimer, Yu. Ivanisenko, A. Mazilkin, B. Straumal, H. Hahn. Mater. Lett. 222, 172 (2018). Crossref
14. X. Zhang, Y. Yu, B. Liu, Y. Zhao, J. Ren, Y. Yan, R. Cao, J. Chen. Journal of Alloys and Compounds. 783, 55 (2019). Crossref
15. G. Korznikova, E. Korznikova, G. Khalikova, K. Nazarov, R. Khisamov, S. Sergeev, R. Shayakhmetov, R. Mulyukov. Lett. Mater. 11 (4s), 533 (2021). Crossref
16. G. Korznikova, E. Korznikova, K. Nazarov, R. Shayakhmetov, R. Khisamov, G. Khalikova, S. Sergeev, R. Mulyukov. Adv. Eng. Mater. 23, 2000757 (2021). Crossref
17. K. Edalati, Sh. Toh, H. Iwaoka, Z. Horita. Acta Materialia. 60 (9), 3885 (2012). Crossref
18. Y. Sun, M. Aindow, R. J. Hebert, T. G. Langdon, E. J. Lavernia. J. Mater. Sci. 52, 12170 (2017). Crossref

19. K. Edalati, S. Toh, M. Watanabe, Z. Horita. Scr. Mater. 66, 386 (2012). Crossref
20. C. O. Ujah, A. P. I. Popoola, O. M. Popoola, V. S. Aigbodion. The International Journal of Advanced Manufacturing Technology. 101, 2275 (2019). Crossref
21. G. Korznikova, R. Kabirov, K. Nazarov, R. Khisamov, R. Shayakhmetov, E. Korznikova, G. Khalikova, R. Mulyukov. JOM. 72, 2898 (2020). Crossref
22. B. B. Straumal, A. R. Kilmametov, Y. Ivanisenko, L. Kurmanaeva, B. Baretzky, Y. O. Kucheev, P. Zięba, A. Korneva, D. A. Molodov. Mater. Lett. 118, 111 (2014). Crossref
23. C. Colinet, A. Pasturel, D. Nguyen Manh, D. G. Pettifor, P. Miodownik. Phys. Rev. B. 56, 552 (1997). Crossref
24. H. Mostaan, F. Karimzadeh, M. H. Abbasi. Thermochimica Acta. 529, 36 (2012). Crossref
25. S. R. Hosseini Zeidabadi, H. Daneshmanesh. Mater. Sci. Eng.: A. 702, 189 (2017). Crossref
26. G. R. Khalikova, G. F. Korznikova, K. S. Nazarov, R. Kh. Khisamov, S. N. Sergeev, R. U. Shayakhmetov, E. A. Korznikova, R. R. Mulyukov. Inorganic Materials: Applied Research. 11 (5), 1409 (2021). Crossref
27. R. Pretorius, A. M. Vredenberg, F. W. Saris. Journal of Applied Physics. 70, 3636 (1991). Crossref
28. R. R. Timiryaev, K. S. Nazarov, G. F. Korznikova, R. R. Kabirov, G. R. Khalikova, R. K. Khisamov, R. U. Shayakhmetov, R. R. Mulyukov. Materials. Technologies. Design. 3 (2), 5 (2021). (in Russian) Crossref
29. B. B. Straumal, A. R. Kilmametov, B. Baretzky, O. A. Kogtenkova, P. B. Straumal, L. Litynska-Dobrzynska, R. Chulist, A. Korneva, P. Zieba. Acta Materialia. 195, 184 (2020). Crossref